The Imprint of Intermittent Interchange Reconnection on the Solar Wind

Peter F. Wyper[1] , C. R. DeVore[2] , S. K. Antiochos[2] , D. I. Pontin[3] , Aleida K. Higginson[2] , Roger Scott[4] ,
Sophie Masson[5,6] , and Theo Pelegrin-Frachon[5]

[1] Department of Mathematical Sciences, Durham University, Durham, DH1 3LE, UK; peter.f.wyper@durham.ac.uk
[2] Heliophysics Science Division, NASA Goddard Space Flight Center, 8800 Greenbelt Road, Greenbelt, MD 20771, USA; c.richard.devore@nasa.gov,
spiro.antiochos@nasa.gov, aleida.k.higginson@nasa.gov
[3] School of Information and Physical Sciences, University of Newcastle, Callaghan, NSW 2308, Australia; david.pontin@newcastle.edu.au
[4] US Naval Research Laboratory, Washington, DC 20375, USA; roger.scott@nrl.navy.mil
[5] Sorbonne Université, Ecole polytechnique, Institut Polytechnique de Paris, Université Paris Saclay, Observatoire de Paris, Université PSL, CNRS, Laboratoire de
Physique des Plasmas (LPP), Paris, France; sophie.masson@lpp.polytechnique.fr, theo.pellegrin@lpp.polytechnique.fr
[6] Observatoire Radioastronomique de Nançay, Observatoire de Paris, CNRS, PSL, Université d'Orléans, Nançay, France

Abstract

The solar wind is known to be highly structured in space and time. Observations from Parker Solar Probe have revealed an abundance of so-called magnetic switchbacks within the near-Sun solar wind. In this Letter, we use a high-resolution, adaptive-mesh, magnetohydrodynamics simulation to explore the disturbances launched into the solar wind by intermittent/bursty interchange reconnection and how they may be related to magnetic switchbacks. We find that repeated ejection of plasmoid flux ropes into the solar wind produces a curtain of propagating and interacting torsional Alfvénic waves. We demonstrate that this curtain forms when plasmoid flux ropes dynamically realign with the radial field as they are ejected from the current layer and that this is a robust effect of the 3D geometry of the interchange reconnection region. Simulated flythroughs of this curtain in the low corona reveal an Alfvénic patch that closely resembles observations of switchback patches, but with relatively small magnetic field deflections. Therefore, we suggest that switchbacks could be the solar wind imprint of intermittent interchange reconnection in the corona, provided an in situ process subsequently amplifies the disturbances to generate the large deflections or reversals of radial field that are typically observed. That is to say, our results indicate that a combination of low-coronal and inner-heliospheric mechanisms may be required to explain switchback observations.

Unified Astronomy Thesaurus concepts: Solar corona (1483); Solar coronal holes (1484); Solar wind (1534); Solar magnetic reconnection (1504); Solar magnetic fields (1503); Solar physics (1476)

Supporting material: animations

1. Introduction

A key discovery made by Parker Solar Probe (PSP) is the high degree of variability of the solar wind within 40 solar radii of the Sun. In particular, a surprisingly high number of radial velocity spikes accompanied by strong drops or reversals of the radial magnetic field component are observed (Bale et al. 2019; Kasper et al. 2019). Such events have become known as magnetic switchbacks.

A number of switchback formation mechanisms have been proposed. One theory is that switchbacks form in situ within the solar wind. This is primarily thought to occur via the steepening of Alfvén waves as the solar wind expands, whereby the WKB evolution of Alfvénic perturbations leads to the inevitable formation of fluctuations of the same order as the ambient field ($\delta B/B \sim \mathcal{O}(1)$; e.g., Völk & Aplers 1973; Barnes & Hollweg 1974; Hollweg 1974). Several simulation studies have demonstrated this mechanism can spontaneously form or help to maintain switchbacks even in a turbulent evolution (Squire et al. 2020; Magyar et al. 2021; Shoda et al. 2021; Johnston et al. 2022). Although promising, this scenario currently fails to explain the spatial clustering and temperature

variations in switchback observations (Kasper et al. 2019; Farrell et al. 2020; Mozer et al. 2020; Woolley et al. 2020; Bale et al. 2021).

Another theory is that coronal interchange reconnection launches kinked field lines outward, which are carried by the solar wind out into the heliosphere as switchbacks (e.g., Fisk & Kasper 2020; Zank et al. 2020). However, an issue with this scenario is that, in the low plasma-β solar corona, such post-reconnection kinked field lines are expected to straighten out under magnetic tension. Simulations of coronal jets, for example, have shown that a deflection of the magnetic field vector of up to 90° is likely the most that could be realized (Karpen et al. 2017; Roberts et al. 2018; Wyper et al. 2018).

Based on 2.5D simulations, Drake et al. (2021) suggested that switchbacks are instead plasmoids ejected from inter-change-reconnecting current layers. This is an appealing prospect, as plasmoid ejection and magnetic switchbacks are both intermittent and spatially localized phenomena. Furthermore, at Lundquist numbers typical of the solar corona, current sheets are highly unstable to plasmoid formation (Loureiro et al. 2007; Wyper & Pontin 2014; Huang & Bhattacharjee 2016). However, it is unclear whether this scenario works in three dimensions, where the tendency is for twist within flux ropes to propagate along the flux-rope axis (e.g., Shibata 1999; Wyper & DeVore 2016).

In this Letter, we present a high-resolution, adaptive-mesh, three-dimensional (3D) magnetohydrodynamics (MHD)
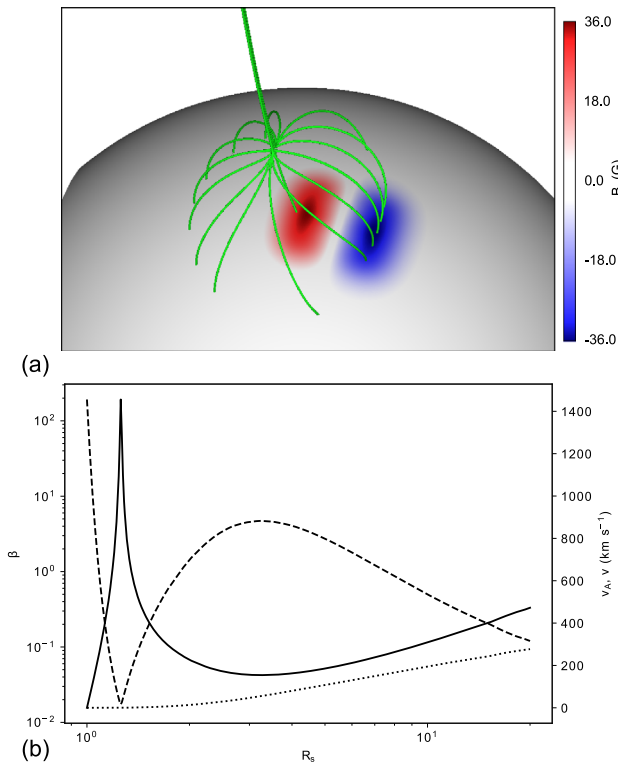
Figure 1. (a) Field lines showing the 3D magnetic null-point topology after the relaxation. (b) Radial profile of the relaxed state showing plasma β (solid line), v_A (dashed), and v_r (dotted).

simulation of interchange reconnection involving intermittent ejections of plasmoid flux ropes. We show that this does not launch radial field reversals typical of switchbacks directly into the solar wind and that this is a generic result of the 3D geometry coupled with the evolution of plasmoid flux ropes as they are ejected from the layer. Instead, Alfvénic structures are produced with characteristics that are remarkably similar to observations of switchback "patches," but with relatively modest magnetic field deflections. We suggest that these waves act as seeds for an in situ mechanism that further steepens them into full radial field reversals while retaining their spatially intermittent nature.

2. Simulation Setup

The simulation was conducted with the Adaptively Refined Magnetohydrodynamic Solver (ARMS; DeVore & Antiochos 2008) in a spherical wedge with $R \in (1R_s, 20R_s)$ and θ, ϕ $\in (-50.4°, 50.4°)$. In the manner of our previous simulations (e.g., Wyper et al. 2021), the ideal MHD equations were solved in spherical coordinates with free-slip conditions on the open side boundaries and free-slip and line-tied conditions on the open top and bottom boundaries, respectively. Magnetic reconnection in the model occurs due to numerical diffusion associated with the convection algorithm. We assume a fully ionized hydrogen plasma, so that $P = 2(\rho/m_p)k_BT$. The temperature is further assumed to be constant and uniform throughout the volume, $T = 1$ MK.

The simulation is initialized with a monopolar ambient magnetic field combined with 16 subsurface magnetic dipoles. The resulting magnetic null-point topology (null height $\approx 1.25R_s$) is shown in Figure 1(a). Such large-scale topologies are often observed above decaying active regions (Nishizuka et al. 2008;

Kumar et al. 2021). However, we note that our results are still broadly applicable to interchange reconnection at considerably smaller scales in the solar corona. The configuration of a 3D magnetic null point surrounded by open-field, low-β plasma is a generic feature within coronal holes, and it occurs down to scales of the smallest coronal jets and bright points (e.g., Zhang et al. 2012; Raouafi et al. 2016). Therefore, the qualitative features of our results should also apply to interchange reconnection occurring at small-scale minority polarities such as those associated with supergranular lanes (e.g., Bale et al. 2021).

The plasma is initialized with a 1D radial Parker wind solution (see Wyper et al. 2021 for the full expression) and the system is evolved until a new dynamic equilibrium is achieved. Profiles for the radial velocity, Alfvén speed, and plasma β along a radial line closely passing the null point are shown in Figure 1(b). The wind reaches $v \approx 300$ km s^{-1} near the open top boundary at $20\,R_s$. This is more typical of slow solar wind speeds, but not dissimilar to the slow speeds measured, for example, in the overly expanded coronal hole sampled by PSP near its first perihelion (e.g., Kasper et al. 2019).

We applied surface motions along contours of B_r in the manner of our previous jet simulations (Wyper et al. 2018) to energize the magnetic field. The driving forms a filament channel in the center of the bipole and expands the field beneath the null point asymmetrically. The asymmetric expansion forms a Sweet–Parker-like spine/fan current layer at the null that lengthens until it becomes violently unstable to the plasmoid instability (Wyper & Pontin 2014).

The simulation grid was allowed to refine adaptively based on gradients in the magnetic field. Here we use the same adaptivity criteria as Wyper et al. (2021), which as shown in Figure 2(a) closely packs the grid blocks—within which reside $8 \times 8 \times 8$ grid cells—around the current layer and associated structures created in the solar wind. In the early phases of the simulation, a maximal grid refinement of 4 was used. As the current layer formed and evolved, the grid refinement was stepped up to the six levels of refinement shown in the figure. The considerable increase in total number of grid cells necessitated that the region of maximal refinement be capped at a radius of 4.5 R_s, above which the grid was limited to the initial maximum of four refinement levels.

Below, in Sections 3 and 4, we focus our analysis on this period of maximal grid refinement. The surface driving was halted well before this period, so that the system is driven solely by the quasi-steady expansion of the filament channel. Thereafter, intermittent reconnection of magnetic flux through the current layer occurs, modulated continually by plasmoid formation and ejection. In what follows, time t is measured from the start of this period.

3. Results

Figure 2(b) shows a cross section of the radial velocity, v_r. An important point to note is that the stagnation point of the plasma flow within the current layer is well below the apex of the inflowing closed field lines (cyan). As a result, some newly opened field lines initially have a strong kink with a reversal of the local radial field component. However, as outlined in the rest of Section 3, we find no evidence that this reversal survives ejection into the wind. Furthermore, many plasmoids are also present, identifiable by their increased plasma density (marked by arrows in Figure 2(c)). Each apparent plasmoid is the cross
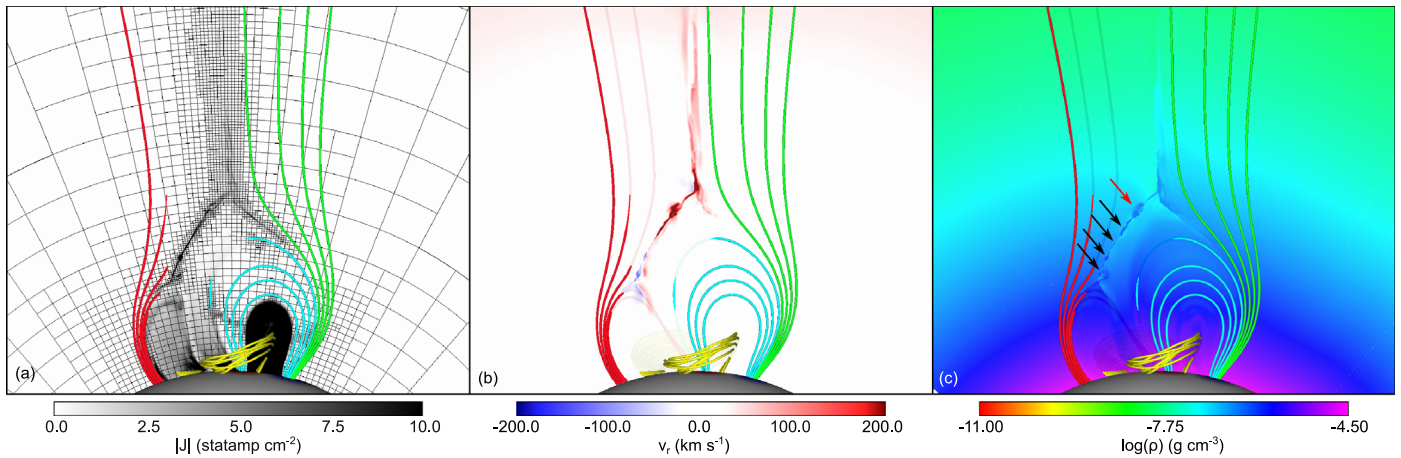
Figure 2. (a) Current density $|J|$ overlaid with the outline of the grid blocks at $t = 1100$ s, (b) v_r, and (c) $\log(\rho)$ highlighting the increased density within the plasmoid flux ropes. Field lines in the filament channel (yellow) and regions of closed inflow (cyan), open inflow (red), and open outflow (green) to/from the current layer are shown for reference. Each panel contains field lines traced in 3D together with the distribution of the corresponding quantity in a vertical plane ($\phi = 1.3°$) that approximately aligns with the reconnection inflows/outflows. An animation of panel (a) is available showing the plasmoid evolution. The duration is 6 s and runs from $t = 0$ to 3600 s.

(An animation of this figure is available.)

section of a small-scale flux rope and, as can be seen from the accompanying animation, they interact and evolve within the layer to produce ubiquitous stochastic small-scale and quasiperiodic large-scale ejections of plasmoids.

One such large-scale plasmoid, with a cross-sectional width several times the width of the current layer, is highlighted with a red arrow in Figure 2(c). Field lines within the plasmoid flux rope throughout its ejection from the layer are shown in Figure 3. The field lines are colored by the local plasma velocity, with yellow sections indicating an ejection speed $v \approx 400$ km s^{-1} (comparable to the inflow Alfvén speed). Within the current layer, the axis of the twisted section of the flux rope is roughly perpendicular to the direction of outflow in Figure 3(a). This alignment agrees with previous 2.5D simulation results (Drake et al. 2021) where in 2.5D the flux ropes appear as magnetic islands. However, beyond this initial stage there are two key differences. First, the twist within the flux rope is localized to a finite length along the flux-rope axis. This should be contrasted with the 2.5D case where the twist is uniform along the (infinite) length of the flux-rope field lines. Second, the flux rope is not disconnected from the open field as it is in 2.5D, rather the plasmoid flux rope has formed by twisting up a section of newly opened field lines. Consequently, on either side of the twisted region, the field lines are more or less straight and aligned to the radial direction where they connect down to the solar surface or out into the solar wind. This field line geometry has a profound effect on how the flux rope behaves as it is ejected.

Figures 3(b)–(d) show that as the plasmoid flux rope runs into the open field at the end of the current layer; the twist within the structure begins to spread along the length of the field lines. As will be further described below in the analysis of the flythrough, this spreading launches a torsional Alfvénic wave. The realignment of the plasmoid flux-rope axis removes the reversal of the radial component previously present within the plasmoid inside the current layer. This is an ideal MHD effect that would be expected to occur independent of which nonideal mechanism creates the flux ropes themselves.

This is the first key result from our simulation. As discussed above, plasmoids within current layers are often pictured as magnetic islands with a guide field that follow an effectively

2.5D evolution. Our results show that in the case of interchange reconnection in a 3D null-point topology, while plasmoids are within the current layer this picture can at least be partially accurate. However, once the plasmoid is ejected from the layer we observe that this 2.5D picture breaks down. At this point in their evolution these are fully 3D flux ropes and they evolve in a fully 3D manner, rotating to become a propagating twist within the solar wind. This demonstrates that the idea that magnetic islands in the 2.5D sense can survive ejection from the current layer is incorrect.

The second key result is that the combined effect of the repeated ejection of plasmoid flux ropes from the current layer is the formation of a curtain of propagating, interacting, torsional Alfvénic waves. Figure 4(a) shows field lines within the ejected flux ropes inside the curtain at time $t = 1600$ s. As the twist within each flux rope propagates upward, new flux ropes are ejected from the current layer into the base of the curtain, replenishing it. Note that the curtain is off to one side of the closed field region due to the twist injected by the driving. The rotating nature of the waves can be seen in the striped reversals of the out-of-plane velocity component shown in Figure 4(b) and the accompanying animation.

Shown in Figure 4(c) is a simulated flythrough at $4 R_s$ (note that above $4.5 R_s$ the coarsening of the grid in our simulation washes out the in situ substructure of the patch). Despite not having a full reversal of the radial field component, in many respects the in situ measurements show a striking similarity with PSP measurements of switchback patches. The encounter can be roughly split into two main phases. In the first part of the encounter, $-7° < \phi < 5°$, the curtain is dominated by Alfvénic waves. There is a sharp rise in $|v|$ as the probe enters the curtain and encounters the most recently opened field lines, before reaching a jagged peak and then tailing off as it passes through. The Alfvénic, weakly compressible nature of the waves is evident from the nearly in-phase peaks of $v_\perp$ and $B_\perp$, the approximately constant overall magnetic field strength $|B|$, and the small variations in ρ in this region. A nearly in-phase increase in v_r with drops in B_r is also evident. The deflections of the magnetic field from the radial direction are contained within this region and peak around $\theta_B \approx 30°$ in this encounter. After leaving this region
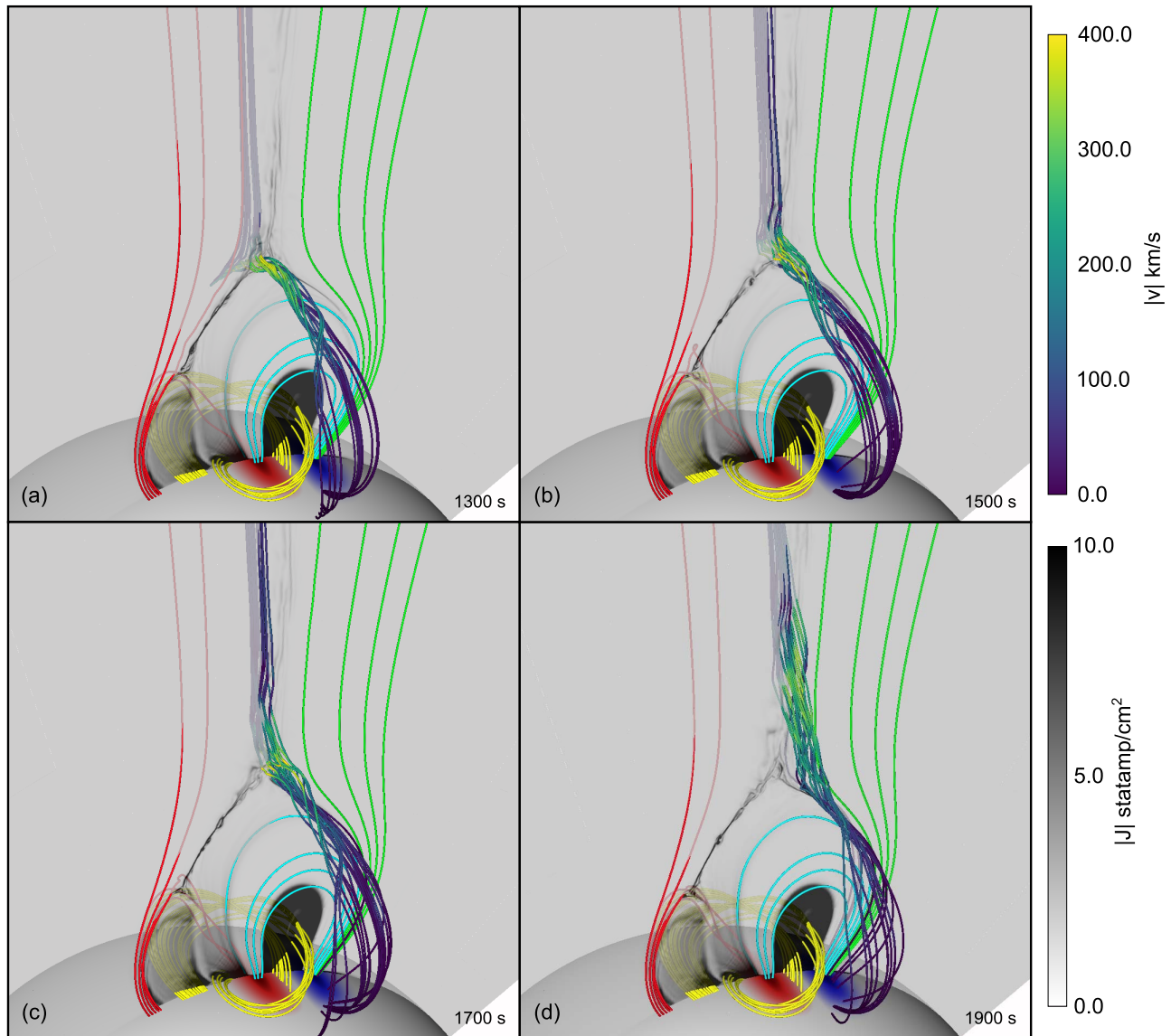
Figure 3. Field lines within the plasmoid flux rope highlighted with the red arrow in Figure 2(c) as it is ejected from the current layer. The field lines are colored (blue/green) according to the local plasma velocity magnitude. Note that the field lines are chosen to show the twist evolution within the flux rope and differ between times. The gray shading shows $|J|$ as in Figure 2(a).

($\phi < -7°$), the probe then encounters a denser region of radial field-aligned flow behind the main curtain. This denser field-aligned flow is a signature of the enhanced density previously present within the plasmoid flux ropes that trails the Alfvénic wave propagation at a lower speed. It forms when the kinks in the field lines propagate away faster than the dense plasmoid plasma as the plasmoid flux ropes are ejected. A similar evolution has been observed in simulations of coronal jets (e.g., Karpen et al. 2017). We tested multiple paths through the curtain and found that this general trend of an asymmetric region of Alfvénic deflections (up to $\theta_B \approx 45°$), followed sometimes by a field-aligned radial flow, was quite robust. In some cases, there are multiple spikes of deflection within the patch, whereas in others a single clean deflection is measured, depending upon how many torsional waves are sampled.

4. Conclusions

In this Letter we have examined the ejection of plasmoids and their signatures in a simulated spacecraft flythrough with a view

to understanding the nature of disturbances launched into the solar wind by intermittent interchange reconnection. Our results show that intermittent interchange reconnection is a continual source of Alfvénic waves. These fluctuations are a direct result of the dynamic realignment toward the radial open field of plasmoid flux ropes as they are ejected from the current layer, which we show is a robust consequence of the 3D geometry of the system. The fluctuations take the form of a curtain of propagating, interacting, torsional Alfvénic waves created by the repeated ejection of plasmoid flux ropes. As the plasmoids are ejected and these waves are launched any local reversal of B_r associated with them is destroyed. The signature of this curtain in the simulated flythrough is an asymmetric patch of radial and transverse velocity spikes, with in-phase drops in radial magnetic field strength and little variation in density or overall magnetic field strength. Within the patch in our simulation the torsional waves also have the same sense of rotation.

Although our system is large scale, our setup is entirely generic, consisting of a 3D null-point topology surrounded by
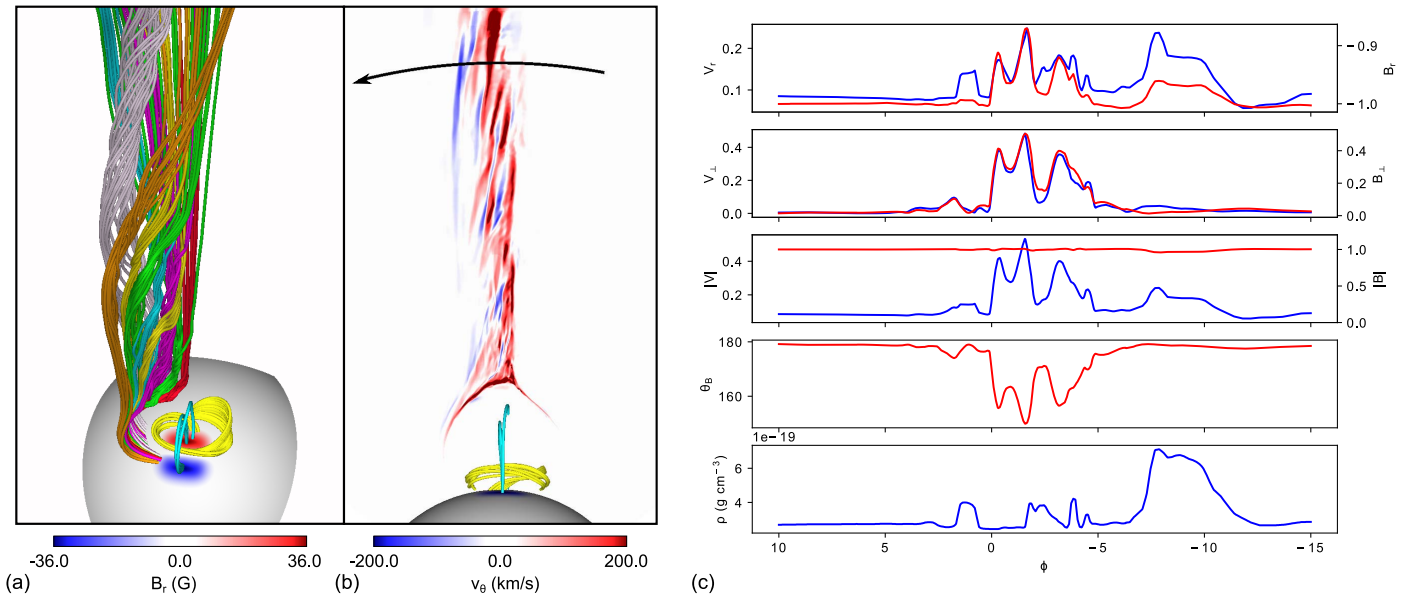
Figure 4. (a) Field lines within the flux ropes forming the curtain at $t = 1600$ s. (b) v_θ in a plane ($\theta = 4°$) aligned with the curtain that approximately bisects the flux ropes. The black line shows the direction and position of the simulated flythrough. (c) Normalized quantities along the flythrough path (from left to right), where $v_\perp = \sqrt{v_\theta^2 + v_\phi^2}$, $B_\perp = \sqrt{B_\theta^2 + B_\phi^2}$, and $\theta_B = \cos^{-1}(B_r/|B|)$. Velocities (blue) and magnetic field components (red) are normalized by the average Alfvén speed (825 km s^{-1}) and total magnetic field strength (0.1527 G), respectively, in the undisturbed wind adjacent to the patch ($\phi \in [5, 10]$). An animation of panel (b) is available showing the evolution. The duration is 6 s and runs from $t = 0$ to 3600 s.

(An animation of this figure is available.)

low plasma-β wind. As such we expect our results to be applicable even to the null-point topologies associated with small-scale minority polarities in, for example, intergranular lanes as has been recently proposed by Bale et al. (2021) to explain the overall patchy nature of switchback observations. Indeed, jet-like flows at or near the ambient Alfvén speed are observed above small-scale polarities in, for example, chromospheric jets (e.g., Tian et al. 2014) and jetlets in plumes (Raouafi & Stenborg 2014). We expect that the qualitative features of our simulation, i.e., the 3D evolution of the plasmoids and the launching of Alfvénic waves (albeit on a smaller scale), should carry over to these smaller events as well, but caution that this requires future 3D modeling efforts to confirm this conjecture. For interchange reconnection occurring above the transition region, however, we expect our results to be generic.

The qualitative features of the simulated flythrough agree well with switchback patches in PSP data (e.g., Bale et al. 2021) except in one important respect: the maximal deflection of the magnetic field direction in our simulation is below what is typically observed. We therefore suggest that switchbacks could be the solar wind imprint of intermittent interchange reconnection in the inner corona, but the large deflections or reversals of radial field that are typically observed must be generated by an amplifying in situ mechanism such as Alfvén wave steepening (e.g., Völk & Aplers 1973). This combination would explain the patchiness that is inherently lacking in current models of expanding turbulence (e.g., Squire et al. 2020) while resolving the challenge of creating perturbations that could survive ejection into and propagation through the low-β solar corona. A testable prediction of this scenario is that switchback deflection angles will reduce on average while still maintaining their patch-like characteristics as PSP orbits progressively closer to the Sun. We look forward with interest to these future observations.

ORCID iDs

Peter F. Wyper ⓘ https://orcid.org/0000-0002-6442-7818
C. R. DeVore ⓘ https://orcid.org/0000-0002-4668-591X
S. K. Antiochos ⓘ https://orcid.org/0000-0003-0176-4312
D. I. Pontin ⓘ https://orcid.org/0000-0002-1089-9270

Aleida K. Higginson ● https://orcid.org/0000-0003-1380-8722
Roger Scott ● https://orcid.org/0000-0001-8517-4920
Sophie Masson ● https://orcid.org/0000-0002-6376-1144
Theo Pelegrin-Frachon ● https://orcid.org/0000-0002-9519-376X

References

Bale, S. D., Badman, S. T., Bonnell, J. W., et al. 2019, Natur, 576, 237
Bale, S. D., Horbury, T. S., Velli, M., et al. 2021, ApJ, 923, 174
Barnes, A., & Hollweg, J. V. 1974, JGR, 79, 2302
DeVore, C. R., & Antiochos, S. K. 2008, ApJ, 680, 740
Drake, J. F., Agapitov, O., Swisdak, M., et al. 2021, A&A, 650, A2
Farrell, W. M., MacDowall, R. J., Gruesbeck, J. R., Bale, S. D., & Kasper, J. C. 2020, ApJS, 249, 28
Fisk, L. A., & Kasper, J. C. 2020, ApJL, 894, L4
Hollweg, J. V. 1974, JGR, 79, 1539
Huang, Y.-M., & Bhattacharjee, A. 2016, ApJ, 818, 20
Johnston, Z., Squire, J., Mallet, A., & Meyrand, R. 2022, PhPl, 29, 072902
Karpen, J. T., DeVore, C. R., Antiochos, S. K., & Pariat, E. 2017, ApJ, 834, 62
Kasper, J. C., Bale, S. D., Belcher, J. W., et al. 2019, Natur, 576, 228
Kumar, P., Karpen, J. T., Antiochos, S. K., et al. 2021, ApJ, 907, 41
Loureiro, N. F., Schekochihin, A. A., & Cowley, S. C. 2007, PhPl, 14, 100703
Magyar, N., Utz, D., Erdelyi, R., & Nakariakov, V. M. 2021, ApJ, 914, 8
Mozer, F. S., Agapitov, O. V., Bale, S. D., et al. 2020, ApJS, 246, 68
Nishizuka, N., Shimizu, M., Nakamura, T., et al. 2008, ApJL, 683, L83
Raouafi, N.-E., & Stenborg, G. 2014, ApJ, 787, 118
Raouafi, N. E., Patsourakos, S., Pariat, E., et al. 2016, SSRv, 201, 1
Roberts, M. A., Uritsky, V. M., DeVore, C. R., & Karpen, J. T. 2018, ApJ, 866, 14
Shibata, K. 1999, Ap&SS, 264, 129
Shoda, M., Chandran, B. D. G., & Cranmer, S. R. 2021, ApJ, 915, 52
Squire, J., Chandran, B. D. G., & Meyrand, R. 2020, ApJL, 891, L2
Tian, H., DeLuca, E. E., Cranmer, S. R., et al. 2014, Sci, 346, 1255711
Völk, H. J., & Aplers, W. 1973, Ap&SS, 20, 267
Woolley, T., Matteini, L., Horbury, T. S., et al. 2020, MNRAS, 498, 5524
Wyper, P. F., Antiochos, S. K., DeVore, C. R., et al. 2021, ApJ, 909, 54
Wyper, P. F., & DeVore, C. R. 2016, ApJ, 820, 77
Wyper, P. F., DeVore, C. R., & Antiochos, S. K. 2018, ApJ, 852, 98
Wyper, P. F., & Pontin, D. I. 2014, PhPl, 21, 082114
Zank, G. P., Nakanotani, M., Zhao, L.-L., Adhikari, L., & Kasper, J. 2020, ApJ, 903, 1
Zhang, Q. M., Chen, P. F., Guo, Y., Fang, C., & Ding, M. D. 2012, ApJ, 746, 19